Islamic Azad University

Journal of
Optoelectronical Nanostructures

Autumn 2021 / Vol. 6, No. 4

Research Paper

Structural, Morphological and Optical Analysis of TiO_2 Thin Films Prepared by RF Magnetron Sputtering

Mohsen Vaezzadeh Asadi[1], Ghahraman Solookinejad[*,1,2], Heydar Izadneshan[1,2]

[1] Department of physics, Marvdasht Branch, Islamic Azad University, marvdasht, Iran

[2] Department of physics, Nanotechnology Research Center, Marvdasht Branch, Islamic Azad University, marvdasht, Iran

Received: 4 Sep. 2021
Revised: 22 Oct. 2021
Accepted: 30 Nov. 2021
Published: 15 Dec. 2021

Use your device to scan and read the article online

Keywords:
Band gap energy, Morphology, RF magnetron sputtering, Tauc's plot, X-ray diffraction

Abstract Thin layer of titanium dioxide has been deposited on a glass sheet using RF magnetron sputtering under different preparation conditions. Phase, lattice parameters, optical features and morphology were investigated under different laboratory conditions in different thicknesses by using XRD, spectrophotometry and atomic force microscopic (AFM), within the visible spectrum range. Also, the lattice structure, in most cases, is tetragonal or a combination of tetragonal and orthorhombic. The band gap energy for each layer was measured using Tauc's Plot. It was observed that the edge of absorption is reduced following an increase in thickness except for a thickness of 75 nm. By increasing the pressure, the band gap energy of the layers or the edge of absorption increases except for 0.04 mbar. By increasing the power, the band gap energy of the layers will change resulting in an increasing-decreasing trend in the edge of absorption, which can be the outcome of changes in the lattice formation.

Citation: Vaezzadeh Asadi M, Solookinejad G. Izadneshan H, Structural, Morphological and Optical Analysis of TiO_2 Thin Films Prepared by RF Magnetron Sputtering, **Journal of Optoelectronical Nanostructures. 2021; 6 (4): 59-94**
DOI: 10.30495/JOPN.2021.28681.1230

***Corresponding author:** Ghahraman Solookinejad
Address: Department of Physics, Marvdasht Branch, Islamic Azad University, Marvdasht, Iran. **Tell:** 00989171893307, **Email:** ghsolooki@gmail.com

1. INTRODUCTION

In the recent years, thin-films of transparent semiconductor have attracted the attention of many researchers due to their high transparency in the visible wavelength range and high electrical conductivity of the layers as well as high reflection in the infrared wavelength region. The usefulness of thin-film properties and the interest in the study of solids behavior have given special attention to thin-films both scientifically and technically [1]. Nowadays, a multitude of modern, sophisticated optical, electrical and electronic components are made of thin films. The thin-film properties of a material are quite different from those of the pile types, especially if the layer thickness is too small. Thin-film technology is used in the production of large-scale [LSI] and very large-scale [VLSI] circuits, which are used to generate, amplify, record and propagate electronic signals. Furthermore, these circuits have been able to improve the memory and increase the speed of data transfer in computers [2]. Various materials such as SnO_2, ZnO, etc. are made and used as thin films in various ways. For example, the SnO_2 layer prepared by RF magnetron sputtering method annealed at 350 – 450° C to detect NOx gas and prepared by active sputtering at 300°C, is suitable for the detection of CO gas. A layer formed by evaporation of tin metal powder in oxygen plasma at different pressures is used to detect ethanol, indicating that the type and method of fabrication are very effective in the functionality and applicability of the layer [3]. One of the most important and widely-used materials in different industries is titanium dioxide or titania, which has natural stability in the form of titanium dioxide [4]. Other applications of the TiO_2 layer are in cosmetics due to having an energy pace of 3.3 to 4.3 eV and its wavelength range is approximately between 365 to 380 nm, denoting that it possesses strong properties in absorbing UV light [5]. If small enough, they would have enough transparency against visible light. Use in thermal mirrors to control the weather of closed places as a combination of TiO_2/Ag/TiO_2 [6] and as anti- reflective coating on devices such as solar cells is another valuable application of this material. It is also used in photocatalyst for water purification [7, 8], hydrogen production [9] and glycerol deformation and degradation [10]. To put it in a nutshell, other applications of this material as a thin-film are in a wide range of industries such as , paper, plastics, enamel, as a catalyst, separators, a coating for self-cleaning surfaces, the white pigment in paints and food coloring[11], biomaterials applications[12,13] and device sensors. In addition to high applications, titanium dioxide is used as a white pigment or in a powder form owing to its high refractive index [14]. Another

important application of titanium dioxide is in solar cells, where these cells can obviate the need for energy by receiving sunlight and converting it into electrical energy and humans can use this clean energy in their industries.

Different solar cells such as silicon solar cells [15], gallium arsenide [16] and more recently, perovskite [17] solar cells have been made using different compositions and layers. Their overall structure is designed to convert luminous energy into electricity from different layers, each of which having a different task. There are many compounds which can be used as anti-reflective coatings on solar cells, the most important ones of which are SiO_2, ZnS, MgF_2, ZnO, and TiO_2 [18]. ZnS and TiO_2 are generally used as materials with high refractive index and SiO_2 and MgF_2 are used as materials with low refractive index. As mentioned, one of the most widely-used materials as an anti-reflective layer in solar cells, especially in perovskite solar cells, is titanium dioxide or titania [19, 20]. Titanium dioxide is available in three main phases of brookite, anatase and rutile [21].

It is very difficult to send size large anatase particles due to the conversion of the anatase phase to rutile with increasing temperature [22]. The n-type titanium oxide thin-film is used as a cathode buffer layer in a variety of solar cells due to its low working function over the indium tin oxide (ITO) substrate. Titanium dioxide is widely used in the visible wavelength range due to its non-toxicity, low cost, high stability, high electron mobility and high transparency [23]. The difference between these crystalline structures can be attributed to the different pressures and heat applied to its formation, which will be investigated in this article. There are various techniques and processes for making titanium dioxide in various ways, including powder, thin-film, and so on, some of which are as follows: spry Pyrolysis [24], Sol-gel [25],Chemical vaporization deposition (CVD) [26],Pulse of laser deposition (PLD) [27] and Radio frequency magnetron sputtering (RF) [28, 29].

Chen explored the basic synthetic methods of nanomaterials and films such as sol/gel, hydrothermal, solvothermal, and microwave [30]. The sol-gel method is a versatile method that can even produce TiO_2 films of amorphous crystals crystalline or low crystallinity at low temperatures [31]. Thermal behavior of TiO_2 thin film is known as one of the main factors regulating morphology. TiO_2 nanostructured films are efficient charge transfer layers [23, 32]. In this paper, titanium dioxide layer, one of the most important layers of solar cells, will be investigated and the effects of laboratory conditions of fabrication of this important layer on its parameters such as phase type, crystallography, lattice parameters, the absorption coefficient, the amount of light transmitted,

morphology and most importantly, the impact on the band gap, which has a direct and significant effect on the efficiency of the solar cells, will be examined. It should be noted that in this paper, deposition has been done based on the RF magnetron sputtering method.

2. MATERIALS AND METHODS

This study used radio frequency Magnetron sputtering device model MSS – MDAU 160 with injection of Argon neutral gas with 99.99% purity. The titanium dioxide tablet had a thickness of 3 mm, a diameter of 76.2 mm and purity of 99.99%. The fixed value of 5 cm was selected as target distance to substrate for deposition. The normal glass substrate of 2 cm × 5 cm was used for deposition.

First, all substrates were washed with distilled water for 15 minutes. Then, the substrates were washed several times with acetone and placed in alcohol for 10 minutes to remove all impurities. Before starting the main deposition on substrates, to purify the vacuum chamber, the initial pressure inside the chamber was set to 3.0×10^{-5} mbar. After adjusting the device and formation of plasma for deposition, a deposition was carried out tentatively for 10 minutes to remove all possible impurities on the target tablet. Having accomplished these stages and ensuring the minimization of the chamber pollution and substrate, a plasma was formed for deposition by regulating the initial power of 500 watts and chamber pressure of 3.0×10^{-5} mbar. During deposition process, the temperature inside the chamber was kept fixed at 58°C. Then, using Argon gas, five thicknesses of TiO_2, (30, 60, 75, 90 and, 105nm) were deposited with a power of 240-watt and 3.0×10^{-2} mbar chamber pressure. In the next step, this thickness was deposited once with 220 watts of power under different chamber pressures for a fixed thickness of 30nm. For the next sample, the chamber pressure was kept at 3.0×10^{-2} mbar and deposition were carried out with different powers. Then, to specify coefficient of absorption and using it to determine the bands gap energy, the layers were lighted by Perkins Elmer model Lambda45. A sample of substrate without coating was placed in the device and its absorption rate became zero for further accurate measurements of substrates with coating. The amount of light absorption and transmission in the transparent layers of (TiO_2) was examined in the range of 320 to 900nm of visible light spectrum. Laboratory samples prepared in the laboratory under different process conditions are shown in Fig. 1.

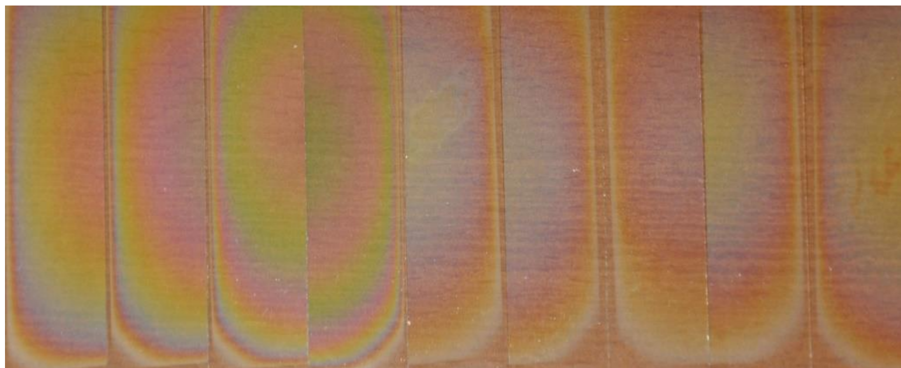

Fig. 1. TiO_2 laboratory samples made in different laboratory conditions add explanation about differences.

3. CHARACTERIZATION

To characterize the titanium dioxide thin film and to investigate the structure of the layers, phase and crystallography and lattice constants, absorption coefficients, transmission rate and finally the band gap were done as follows. In order to do the research, The D8 advanced Bruker X-ray diffraction spectrometer with a wavelength of 1.54 angstrom kα - cu made in Germany was used. The X-ray scattering spectrum was taken in the 2θ intervals from 10.000 to 80.000 angle at 0.050 deg. and at 1 second intervals at room temperature of 25°C.

3.1. ABSORPTION COEFFICIENT AND TRANSMISSION RATE

Perkins Elmer model Lambda 45 was used so as to light the layers, in a way that an uncoated substrate sample was inserted into the device, the absorbance of which was set to be zero for subsequent accurate measurements of the substrates containing the coating. Lighting was done on layers made in the range of 320 – 900nm visible light and the absorbance of the layers was extracted. Then, we were calculated the coefficient of absorption and the percentage of light transmittance of each layer by using (1) and (2), respectively.

$$\alpha = (2.303)\, A/t \tag{1}$$

and

$$\%T = \exp(-\alpha t) \tag{2}$$

Where α is the coefficient of absorption, A absorption rate and t the thickness of the layer, respectively.

There are different methods such as Beer-Lambert law [33] and Tauc's plot [34] for calculating band gap energy. In this research we used Tauc's plot method. Coefficient of absorption which term in (3) can be described based on a function of photon energy (eV). Using (3), we calculated the band gap energy.

$$\alpha h\nu = (E_g - h\nu)^n \tag{3}$$

Where h is the Planck's constant, ν is the frequency, n is the numerical value depending on transition nature having values of 1/2, 2, and 3/2 for direct, indirect and forbidden transition, respectively. considering that TiO_2 is a semi-conductor with direct band gap transition, the value of 1/2 was considered for n [35]. Therefore, with drawing $(\alpha h\nu)^2$ versus hν and extrapolation of the linear area of the curve in $\alpha = 0$, direct bands gap energy for titanium dioxide was calculated.

4. RESULTS AND DISCUSSION

4.1. STRUCTURE, PHASE, CRYSTALLOGRAPHY AND LATTICE CONSTANT

4.1.1. TiO_2 LAYER MADE WITH DIFFERENT THICKNESSES

Titanium dioxide layers with different thicknesses were made under 240-watts power and pressure and pressure 3.5×10^{-2} mbar. The XRD spectrum pattern for different thicknesses was obtained according to Fig 2.

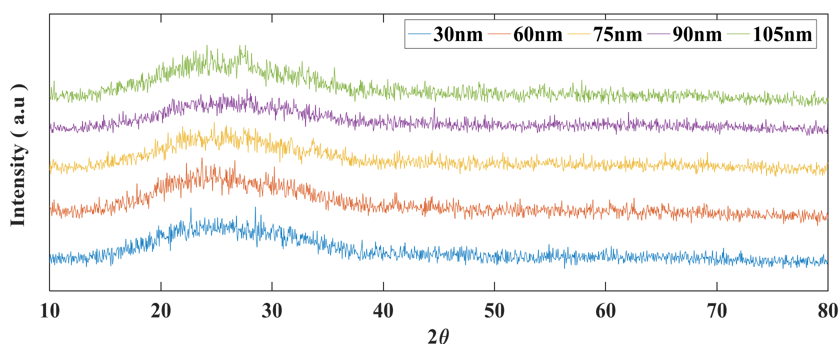

Fig. 2. XRD pattern TiO_2 thin film with thicknesses of (a) 30nm, (b) 60nm, (c) 75nm, d) 90nm, and (e) 105nm

Fig. 2, shows that the constituent layers are all amorphous and the polycrystalline lattice structure is all tetragonal. Bange *et al.* [36] and Williams *et al.* [37] observed amorphous crystal transfer at 350 – 400°C for RF film vaporization and sputtering, respectively, all of which having a mixed phase of rutile and anatase, and this mixed phase has been observed by other individuals

and no brookite phase has been seen. Suhail et al. have observed a mixed phase of rutile and anatase for TiO_2 layer by DC reactive magnetron sputtering method [38]. Schiller *et al.* observed reactive anatase at the substrate temperature of 25 – 500°C [39] with DC reactive plasmatron sputtering and Pawlewicz and Bush [40] observed the mixed phase of rutile/anatase at the substrate temperature of 200 – 500°C. Mardare *et al.* [41] and Hou [42] reported a thin-film TiO_2 prepared with mixed phase of rutile and anatase by DC magnetron sputtering and magnetron sputtering cooked in the temperatures of 300 – 1000°C. The results gained from the deposition with different thicknesses under the constant power and constant pressure are summarized in the (I).

The unit cell parameters of TiO_2 anatase tetragonal structure were calculated. The average values of lattice parameters are found to be a = 3.700 A^0 and c = 9.560 A^0. They are very close to lattice parameters calculated from other experimental data.

TABLE I
RESULTS OF THE DEPOSITION WITH DIFFERENT THICKNESSES

Thickness(nm)	crystallography	Lattice structure	Phase	Lattice const.(A^0)	
				a = b	c
30	Amorphous	Tetragonal	Anatase	3.785	9.539
			Rutile	4.580	2.95
60	Amorphous	Tetragonal	Anatase	3.730	9.370
			Rutile	4.593	2.958
75	Amorphous	Tetragonal	Anatase	3.775	9.420
			Rutile	4.580	2.950
90	Amorphous	Tetragonal	Anatase	3.730	9.370
			Rutile	4.593	2.959
105	Amorphous	Tetragonal	Anatase	3.783	9.510
			Rutile	4.593	2.959

4.1.2. LAYER MADE IN DIFFERENT PRESSURES

Titanium dioxide layers with constant thicknesses 30nm were made under 220-watts power and different pressures. The pattern of the XRD spectrum is shown in Fig 3.

Fig. 3 depicts, show that the constituent layers are all amorphous. The layer made at a pressure of 3.0×10^{-2} mbar has an orthorhombic/tetragonal lattice structure, the phase of which is a combination of anatase/srilankite.

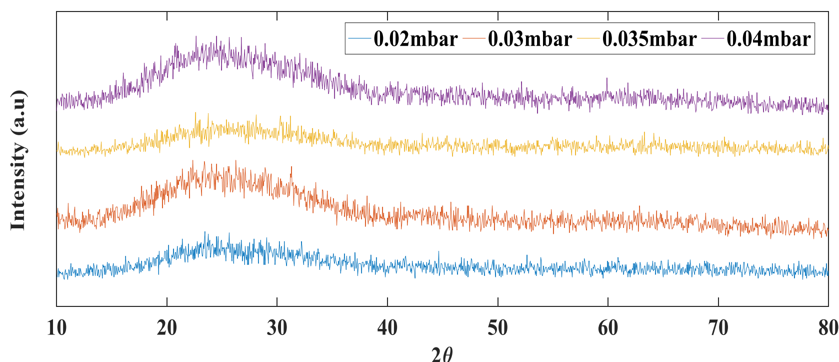

Fig. 3. XRD pattern TiO_2 layers made at pressures of (a) 2.0×10^{-2}, (b) 3.0×10^{-2}, (c) 3.5×10^{-2}, and (d) 4.0×10^{-2} mbar

The layer, made at 3.5×10^{-2} mbar, has a crystal structure of mixed Ti_3O_5, orthorhombic and tetragonal and the lattice structure of which is a mixture of monoclinic Ti_3o_5, anatase and rutile TiO_2 and the other layers made have a tetragonal structure and have a mixed phase of rutile and anatase [38]. Nair *et al.* [43] reported the mixed phase of rutile and anatase for titanium dioxide thin films made by RF magnetron sputtering at different pressures. Crystalline TiO_2 (anatase, rutile or a mixture of both) was obtained either by controlling the gas flow and sputtering pressure [44,45]. The results obtained from the constant thickness deposition under constant deposition power of 220 watts and different pressures are summarized in (II).

TABLE II
RESULTS OF THE DEPOSITION UNDER DIFFERENT PRESSURES

Pressure(mbar)	crystallography	Lattice structure	Phase	Lattice const.(A^0) a = b	c
2.0×10^{-2}	Amorphous	Tetragonal	Anatase	3.785	9.514
			Rutile	4.593	2.958
3.0×10^{-2}	Amorphous	Tetragonal	Anatase	3.783	9.510
		Orthorhombic	Srilankite	4.550	4.920
3.5×10^{-2}	Amorphous	Tetragonal	Anatase	3.730	9.370
			Rutile	4.580	2.950
		monoclinic	Ti_3O_5	10.120	9.970
4.0×10^{-2}	Amorphous	Tetragonal	Anatase	3.730	9.370
			Rutile	4.580	2.950

4.1.3. LAYER MADE IN DIFFERENT POWERS

Titanium dioxide layers with constant thicknesses 30nm were made under constant pressure 3.5×10^{-2} mbar and different powers. The pattern of the XRD spectrum is shown in Fig 4.

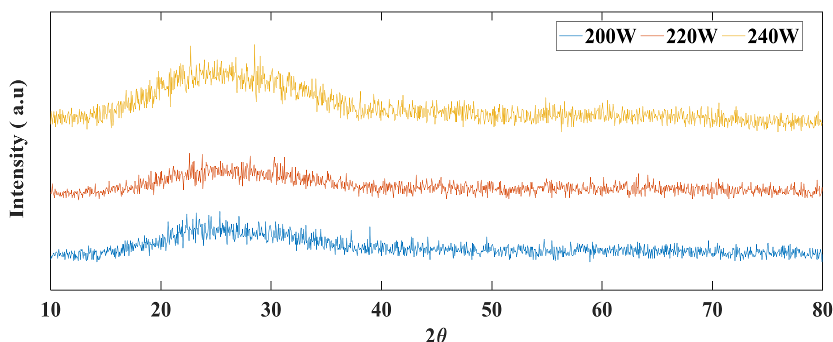

Fig. 4. XRD pattern TiO_2 layers made at pressures of (a)2.0×10^{-2}, (b) 3.0×10^{-2}, (c) 3.5×10^{-2}, and (d) 4.0×10^{-2} mbar

Fig. 4 shows that the constituent layers are all amorphous. The layer made at the power of 200 watts has an orthorhombic/tetragonal lattice structure, the phase of which is a combination of brookite/rutile. The layer made at 220 watts power has a lattice structure of monoclinic Ti_3O_5, and tetragonal, the phase of which is a mixture of anatase/rutile. Also, the layer made at 240 watts has a lattice structure of tetragonal, the phase of which is a mixture of anatase/rutile. In fact, the structure and phase change with the change of deposition power and move towards more homogeneity. This is easily explained by the fact that more RF power was employed, which increased the sputtering yield, and a considerably higher vacuum, which increased the mean free path of our atoms/ions [46]. The results obtained from the constant thickness deposition of 30 nm under different power of deposition are illustrated in (III).

The unit cell parameters of TiO_2 anatase and rutile tetragonal structure were calculated. The average values of lattice parameters under different preparation condition are shown in (IV). They are very close to lattice parameters calculated from other experimental data.

TABLE III
RESULTS OF DEPOSITION UNDER DIFFERENT POWER

Power(W)	Crystallography	Lattice structure	Phase	Lattice const.(A^0) a	b	c
200	Amorphous	Orthorhombic	Brookite	9.182	5.456	5.143
		Tetragonal	Rutile	4.593	4.593	2.959
220	Amorphous	Monoclinic	Ti_3O_5	10.120	5.074	9.970
			Anatase	3.730	3.730	9.370
		Tetragonal	Rutile	4.580	4.580	2.950
240	Amorphous	Tetragonal	Anatase	3.785	3.785	9.514
			Rutile	4.580	4.580	2.950

TABLE IV
VARIOUS VALUES OF STRUCTURAL PARAMETERS OF ANATASE, RUTILE AND BROOKITE

	a = b(A^0)	c(A^0)	c/a
This work			
Diff. thicknesses			
Anatase	3.760	9.442	2.511
Rutile	4.588	2.955	0.644
Diff. pressures			
Anatase	3.757	9.441	2.513
Rutile	4.584	2.953	0.644
Diff. powers			
Anatase	4.584	9.442	2.060
Rutile	4.584	2.953	0.644
Brookite	a = 9.182, b = 5.456	5.143	0.560
Experiments of other			
Anatase			
	3.733[47]	9.372[47]	2.510[47]
	3.782[48]	9.502[48]	2.512[48]
	3.823[49]	9.612[49]	2.514[49]
	3.814[50]	9.583[50]	2.512[50]
	3.787[51]	9.516[51]	2.513[51]
Rutile			
	4.522[47]	2.905[47]	0.642[47]

	4.593[48]	2.959[48]	0.644[48]
	4.534[52]	2.920[52]	0.644[52]
	4.631[53]	2.980[53]	0.643[53]
Brookite			
	a = 9.184, b = 5.447 [49]	5.145[49]	0.560[49]

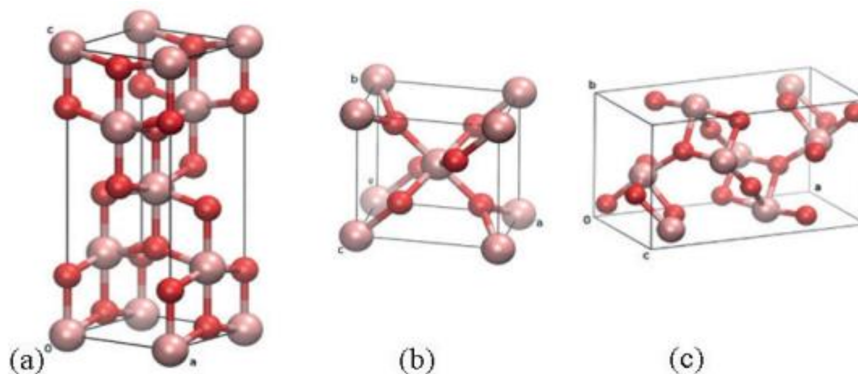

Fig. 5. Crystal structures of TiO_2 (a) anatase, (b) rutile and (c) brookite

calculated values of lattice parameters a, c and the quotient c/a, as well as other theoretical and experimental values, are given in (IV). We found that our optimized lattice parameters are in good agreement with experimental other obtained results.

5. ATOMIC FORCE MICROSCOPIC(AFM)

Surface roughness and topography used to characterize contact surfaces, are described with surface roughness [54]. In practice, most commonly used parameters for surface roughness description are R_a, R_{rms}, and R_{max}. Average surface roughness, R_a, gives a very good overall description of height variations, but does not give any information on the wavelength and is not sensitive to small changes in profile. Root mean square, R_{rms}, is more sensitive to deviations from the main line than R_a [55,56]. The surface roughness of transparent conductive thin films has a significant influence on device performance [57].
The Figs. (6,7), and (8) show the microstructure of the TiO_2, which are made under different conditions deposition. Atomic force microscopy (AFM) analysis was done using Mobile(s) equipment, and the topography contrast images were acquired in the contact mode. The grain-wise identification and profile statistics were carried on using Gwyddion 2.31 software.

5.1. THICKNESS – ROUGHNESS RELATION

At this stage, the layers of titanium dioxide prepared in different thicknesses at a constant sputtering power of 240W and sputtering pressure of 0.035mbar were examined by atomic force microscopy. The images and results are shown in Fig. 6 and (V), respectively.

(a)

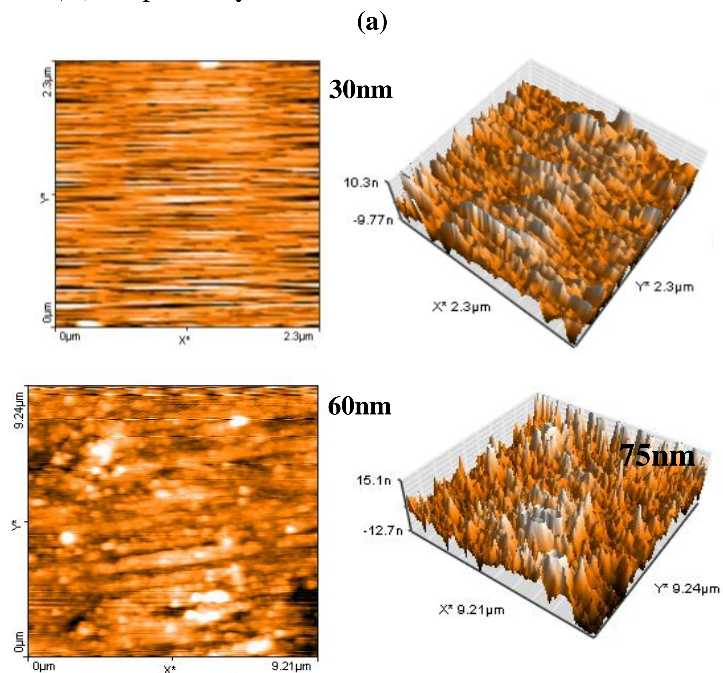

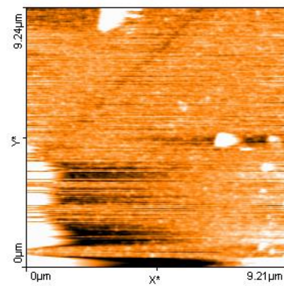

75nm

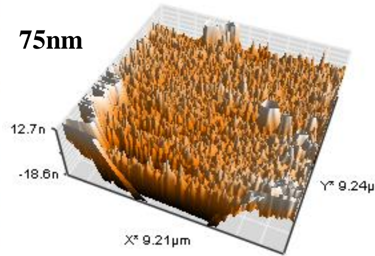

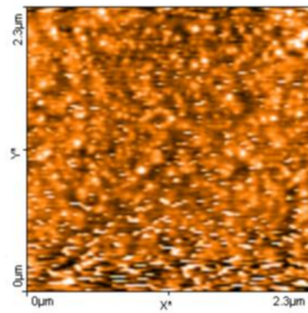

90nm

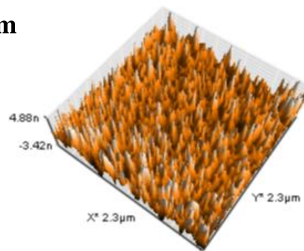

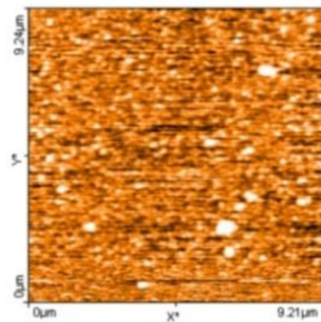

105nm

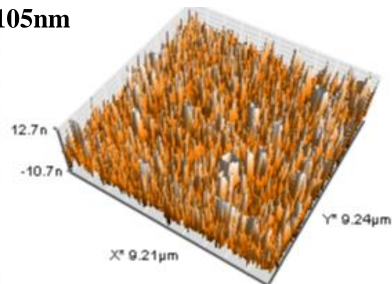

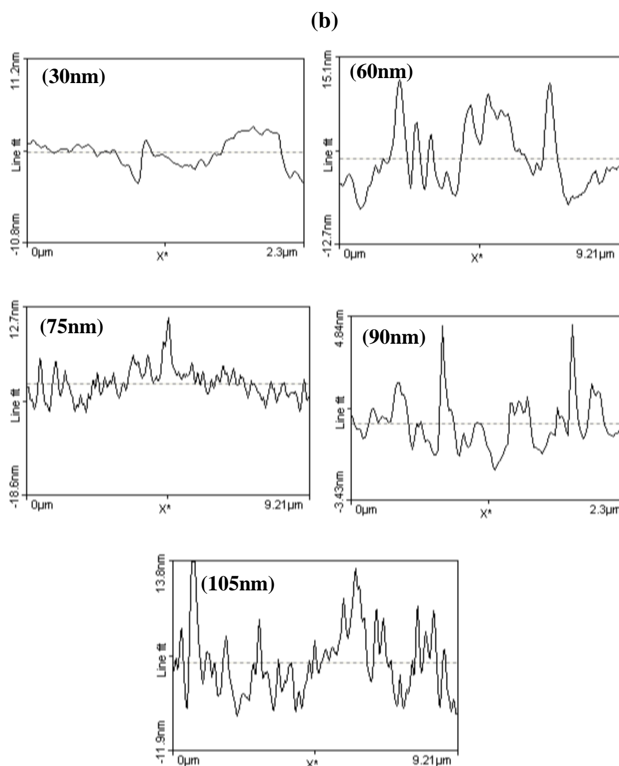

Fig. 6. (a) Typical 2D and 3D AFM images and (b) Typical roughness analysis of TiO_2 thin films made in different thicknesses.

TABLE V
ROUGHNESS PARAMETERS OF TiO_2 THIN FILMS MADE IN DIFFERENT THICKNESSES

		Thickness(nm)				
		30	60	75	90	105
parameter	Average roughness(nm)	0.9045	0.8311	0.7481	0.7028	0.8185
	Median roughness	0.9686	0.8863	0.8314	0.7098	0.8941
	Minimum roughness(nm)	0.3216	0.1882	0.0000	0.1765	0.0000
	Maximum roughness(nm)	1.0000	0.9882	0.9882	1.0000	0.9882

R_a (nm)	0.0971	0.1513	0.2253	0.1621	0.1665
R_q (nm)	0.1278	0.1722	0.2601	0.1898	0.2021
R_q/R_a	1.316	1.138	1.154	1.170	1.214
R_{sk}	-1.82	-0.716	-0.766	-0.189	-1.18
R_{ku}	3.08	-0.611	-0.566	-0.977	0.729

It is observed that the maximum roughness varied in the range of 0.9882 to 1.0000nm with the thickness change. The roughness analysis of TiO_2 thin films is presented in Fig. 6. With an increase in the thickness, roughness initially increased (up to 75 nm) and then decreased and increased again to a thickness of 105 nm. The same behavior was true for R_q. The topography and section analysis of TiO_2 thin films with different thickness obtained by AFM images are listed in (V). It can be seen that the average roughness almost decreased as the thickness increased.

5.2. EFFECT OF SPUTTERING PRESSURE

Next, the layers of titanium dioxide, prepared with constant thickness of 30nm at a constant sputtering power 220W, were examined under different sputtering pressures by atomic force microscopy. The images and results are shown in Fig. 7 and (VI), respectively.

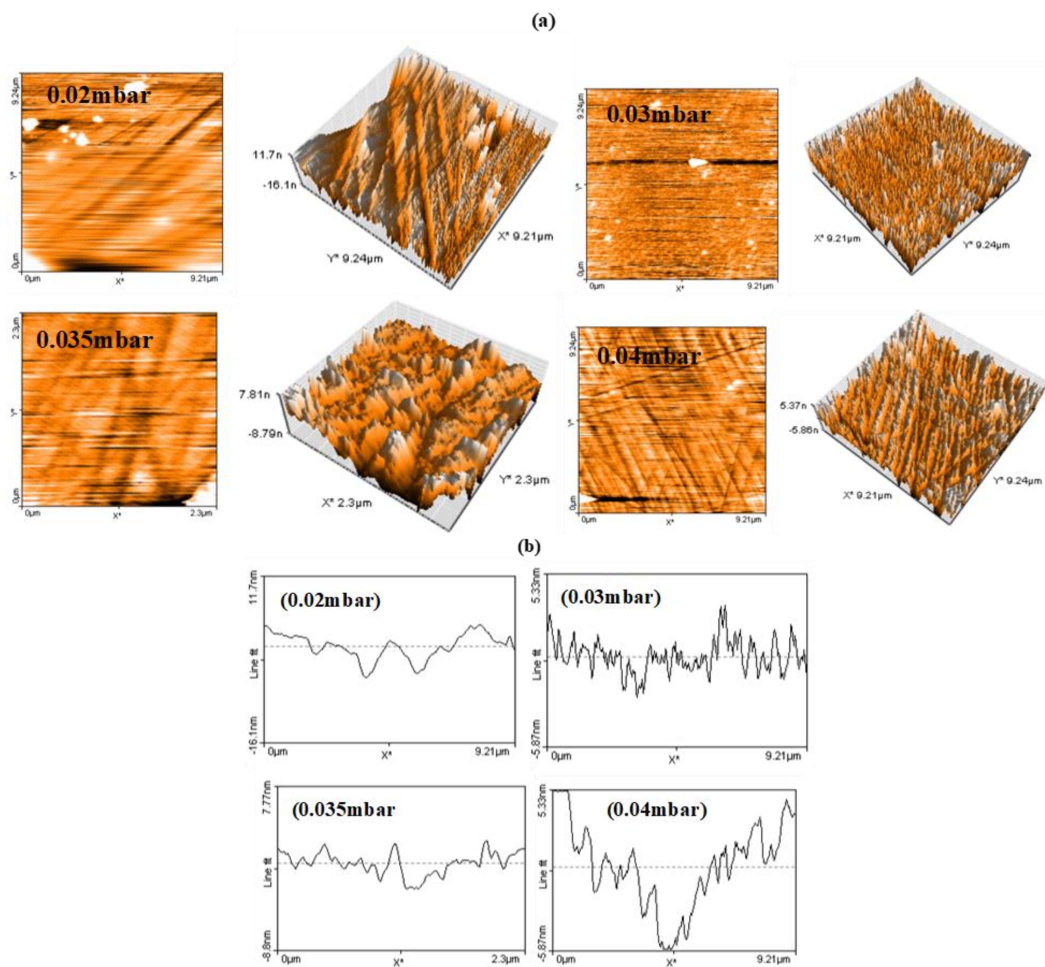

Fig. 7. (a) Typical 2D and 3D AFM images and (b) Typical roughness analysis of TiO_2 thin films made under different sputtering pressures

TABLE VI

Roughness parameters of TiO_2 thin films made under different pressures

		Pressure(mbar)			
		0.02	0.03	0.035	0.04
Parameter	Average roughness(nm)	0.9045	0.8311	0.7481	0.7027
	Median roughness	0.9686	0.8863	0.7314	0.7098
	Minimum roughness(nm)	0.3216	0.1882	0.0000	0.1765
	Maximum roughness(nm)	1.0000	0.9882	0.9882	1.0000
	R_a (nm)	0.0971	0.1513	0.2253	0.1621
	R_q (nm)	0.1287	0.1722	0.2601	0.1898
	R_q/R_a	1.316	1.138	1.154	1.170
	R_{sk}	-1.82	-0.716	-0.766	-0.189
	R_{ku}	3.08	-0.611	-0.566	-0.977

It is evident that the maximum roughness varies in the range 0.9882 to 1.0000 nm with the pressure change. The roughness analysis of TiO_2 thin films is presented in Fig. 7. Initially, roughness increases and then decreases following an increase in pressure up to 0.03 mbar. The same behavior is true for R_q. The topography and section analysis of TiO_2 thin films under different pressures obtained by AFM images are listed in (VI). It can be gathered that the average roughness almost decreased with increase of pressure.

5.3. EFFECT OF SPUTTERING POWER

At this stage, layers of titanium dioxide, prepared in constant thicknesses of 30nm, were examined at a constant sputtering pressure of 0.035mbar and different sputtering powers. The images and results are shown in Fig. 8 and (VII), respectively.

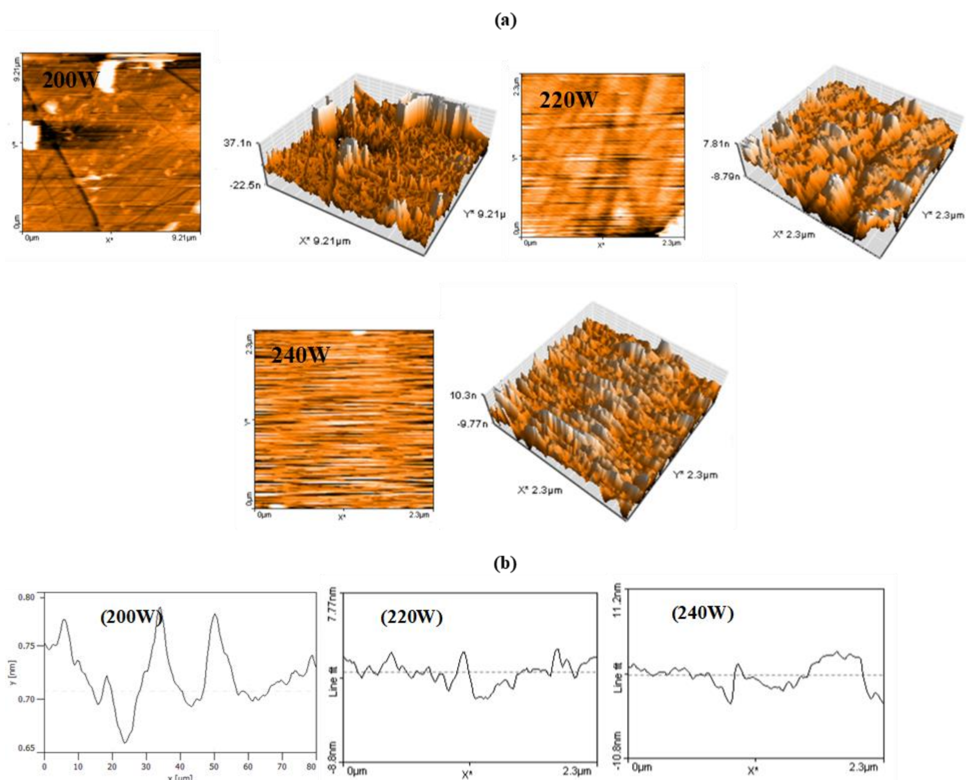

Fig. 8. (a) Typical 2D and 3D AFM images and (b) Typical Roughness analysis of TiO_2 thin films made in different sputtering powers

Table VII
Roughness parameters of TiO_2 thin films made in different sputtering powers

		Power (W)		
		200	220	240
Parameter	Average roughness(nm)	0.7236	0.8862	0.9045
	Median roughness	0.7373	0.9686	0.9686
	Minimum roughness(nm)	0.0000	0.1333	0.3216
	Maximum roughness(nm)	0.9882	1.0000	1.0000

	R_a (nm)	0.1044	0.1207	0.0971
	R_q (nm)	0.1429	0.1690	0.1287
	R_q/R_a	1.368	1.400	1.316
	R_{sk}	-0.94	-2.21	-1.82
	R_{ku}	2.34	4.78	3.08

It is obvious that the maximum roughness varies within 0.9882 to 1.0000 nm with the pressure change. The roughness analysis of TiO_2 thin films is presented in Fig. 8. The amount of roughness variation after increasing the power of the deposition system is negligible. The same process is true for R_q. The topography and section analysis of TiO_2 thin films under different powers obtained by AFM images are listed in (VII). Moreover, it can be reported that the average roughness rose with increase of power. Measuring the surface roughness of TiO_2 films was important before the manufacturing of photoelectric devices. The roughness parameters were estimated by the analyzing the topography scans of the sample's surface. The surface profile parameters include average roughness, R_a, root mean square roughness, R_q, skewness of the line, R_{sk}, and kurtosis of the line, R_{ku}. The average roughness, R_a, is the mean height as calculated over the entire measured length/area. Ra is typically used to describe the roughness of machined surfaces. It is useful for detecting general variations in overall profile height characteristics and for monitoring an established manufacturing process.

Root mean square (RMS) roughness, R_q, is the square root of the distribution of surface height and is considered to be more sensitive than the average roughness for large deviations from the mean line/plane and is also used in computing the skew and kurtosis parameters. RMS roughness, R_q, describes the finish of optical surfaces. It represents the standard deviation of the profile heights and is used in computations of skewness and kurtosis. R_{sk} is used to measure the symmetry of the variations of a profile/surface about the mean line/plane and is more sensitive to occasional deep valleys or high peaks.

R_{sk} illustrates load carrying capacity, porosity, and characteristics of non-conventional machining processes. Negative skewness is a criterion for a good bearing surface. Usually, R_{sk} is used to distinguish two profiles of the same R_a or R_q values but of different shapes. Kurtosis is a measure of the distribution of spikes above and below the mean line. Kurtosis describes machined surfaces and is rarely used for optical surfaces. It is sometimes specified for the control of stress fracture. R_{ku} is used to measure the distribution of the spikes above and below the mean line/plane. For spiky surfaces, $R_{ku} > 3$; for bumpy surfaces, R_{ku}

< 3; and perfectly random surfaces have kurtosis 3. For a Gaussian distribution of asperity height, statistical theory shows that the ratio R_q/R_a, should be 1.25. Ward [58] notes that the asperity height distribution of most engineering surfaces may be approximated by a Gaussian distribution with R_q/R_a values of up to 1.31. (V), (VI) and, (VII) show the roughness parameters for layers made under different deposition conditions. Project area for samples was selected 852.1 μm^2 as well inclination θ and φ selected 0.0 and 59.5 degrees, respectively. The values of R_q/R_a, using data collected from AFM imaging for (V), 1.138 - 1.316, (VI), 1.279 - 1.404 and (VII), 1.316 - 1.400 are reasonably close to the value of 1.31 predicted by theory.

This result is significant since it indicates that at the imaging scale, the asperity height distribution of these surfaces is approximately Gaussian and that the statistical relationships for surface roughness are applicable.

In (V), (VI) and, (VII), negative values of the skewness indicate that the valleys are dominant over the scanned area and positive values show that the peaks are dominant on the surface. Continued negative values would indicate cracks, representative of valleys. The distribution of positive and negative values indicates the existence of protruding grains. For Kurtosis, $R_{ku} < 3$ shows that the distribution over the scanned area has relatively few high peaks and low valleys, which means a bumpy surface. When $R_{ku} > 3$, the distribution will have relatively higher numbers of high peaks and low valleys, characteristic of a spiky surface [59]. The results of skewness and kurtosis prove that the surface of TiO_2 thin films is generally spiky with peaks being dominant. Films with high R_{ku} values have high R_t and R_z values as well. This is due to the strong relation between these parameters, where R_{ku} is, mathematically, directly related to the peak heights and valley depths [60,61].

6. ABSORPTION COEFFICIENT AND TRANSMISSION SPECTRUM

6.1. DEPENDENCE ON THE THICKNESS

Fig. 9-a and Fig. 9-b, summarize the absorption coefficients and transmission spectrum in terms of a function of the wavelength of the visible spectrum of light drawn for different thicknesses compared with each other.

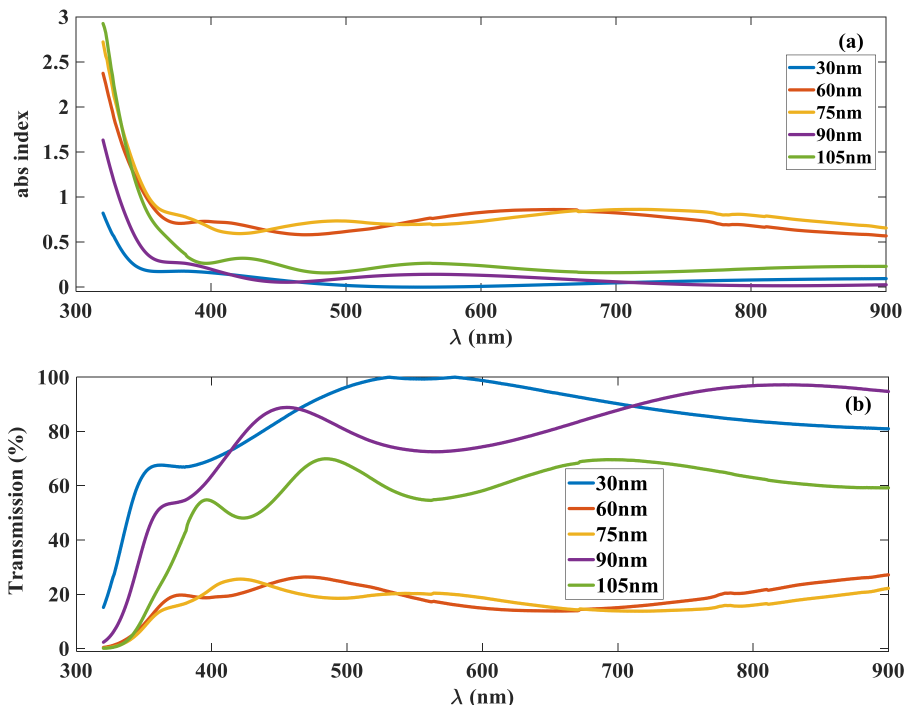

Fig. 9. (a) Absorption coefficient, (b) Transmission spectrum in different thicknesses

Fig. 9-a and Fig. 9-b, show the changes rate of absorption coefficient and the transmission spectrum of each layer in terms of wavelength in the visible light range, respectively. Due to the high absorption coefficient of titanium dioxide in the visible light range, it drops significantly for wavelengths below 400 nm (λ<400 nm). Hou [42] reported 80 to 85(%) transmittances for titanium dioxide thin films made by magnetron sputtering. It is quite clear that the 30 nm and, 90 nm layers have the lowest absorption coefficient and the highest transmission spectrum between 80 to 90(%) between different thicknesses in the range 420 to 700 nm, which is suitable for solar cells of all thicknesses. In the rest of the layers, approximately the highest light transmission spectrum (minimum absorption) occurs in the wavelength range of 400 to 550 nm

.

6.2. DEPENDENCE ON SPUTTERING PRESSURE

Fig. 10-a and Fig. 10-b, represent the absorption coefficients and the amount of light transmission spectrum in terms of the wavelength range of the visible light spectrum plotted for 30nm thickness made under different pressures.

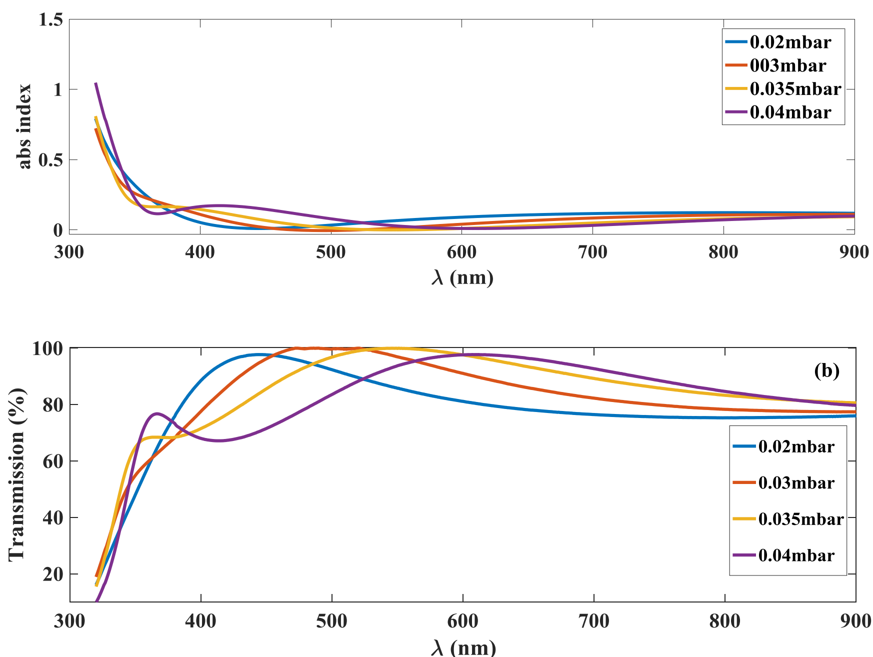

Fig. 10. (a) Absorption coefficient, (b) Transmission spectrum in different sputtering pressures

Fig. 10-a and Fig. 10-b, display the changes rate of absorption coefficient and the transmission spectrum of each layer in terms of wavelength in the visible light range, respectively. The amount of light transmitted is almost the same in all the layers, but with a slight difference, as shown in the Fig. 10-b, the 30nm layer made under the pressure of 3.0×10^{-2}mbar has the highest transmittance (lowest absorption coefficient) among the various layers.

As seen in Fig. 10-b, it could be concluded that the pressure change in the layer construction, changes the wavelength range of the maximum transmitted light, in a way that for the layers made at pressures of 2.0×10^{-2} and 3.0×10^{-2} mbar, the highest wavelength light transmittance occurs at 400 to 500nm and at 3.5×10^{-2} and 4.0×10^{-2}mbar, occurring at 450 to 550nm and 550 to 650nm, respectively. In general, the highest light transmittance (lowest absorption) occurs in layers at wavelengths of 400 to 650nm. Therefore, the change in layer pressure changes the light transmittance to create the maximum wavelength layer, or as the device layer pressure increases, the higher (having lower energy) wavelengths have a greater share of the crossing.

6.3. DEPENDENCE ON SPUTTERING POWER

Fig. 11-a and Fig. 11-b, illustrate the absorption coefficients and the amount of light transmitted over the wavelength range of the visible spectrum of light drawn for the 30 nm layers made under different powers.

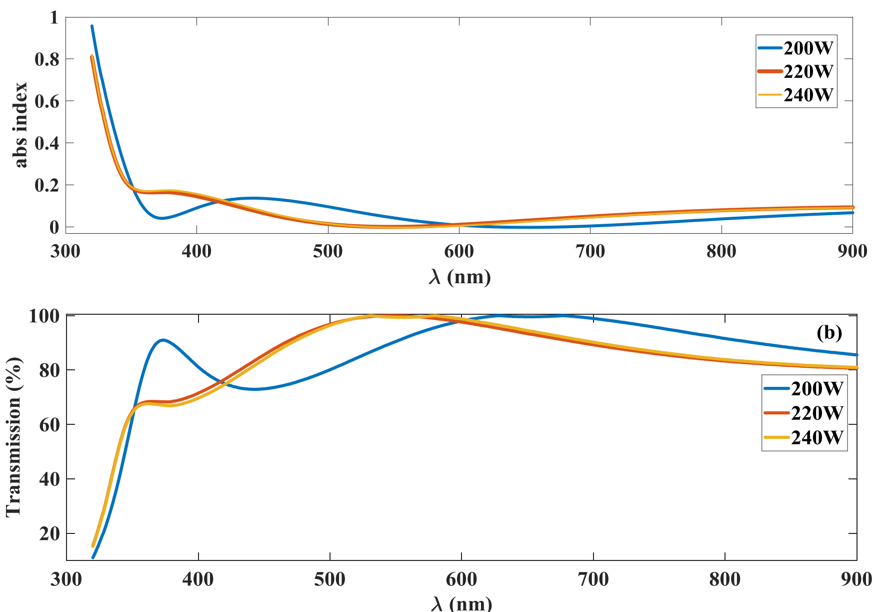

Fig. 11. (a) Absorption coefficient, (b) Transmission spectrum in different sputtering powers.

Fig. 11-a and Fig. 11-b, show changes rate of absorption coefficient and the transmission spectrum of each layer in terms of wavelength in the visible light range, respectively. The amount of light transmitted as well as the range of their maximum wavelength transmittance in all the layers is almost the same, and only the wavelength transitions of the layers different, in a way that in the fabricated layers, the highest amount of transmission (lowest absorption) at 220 and 240 watts, which is overlapping of course, is in the range of 450 to 600nm, and the layer made at 200 watts is in the range of 600 to 700nm. Therefore, it can be concluded that a change in the deposition power of the layer construction changes the range of the wavelength of the maximum transmitted light. In other words, with an increase in the deposition power, more energetic (shorter wavelengths) light has more transmission and more wavelengths also contribute to maximum light transmission.

7. DETERMING BAND GAP ENERGY (E_G)

The final results of extraction of bands gap energy of the making layers under different preparation conditions by using Figs. 12-a, 12-b, and 12-c, are shown in (VIII).

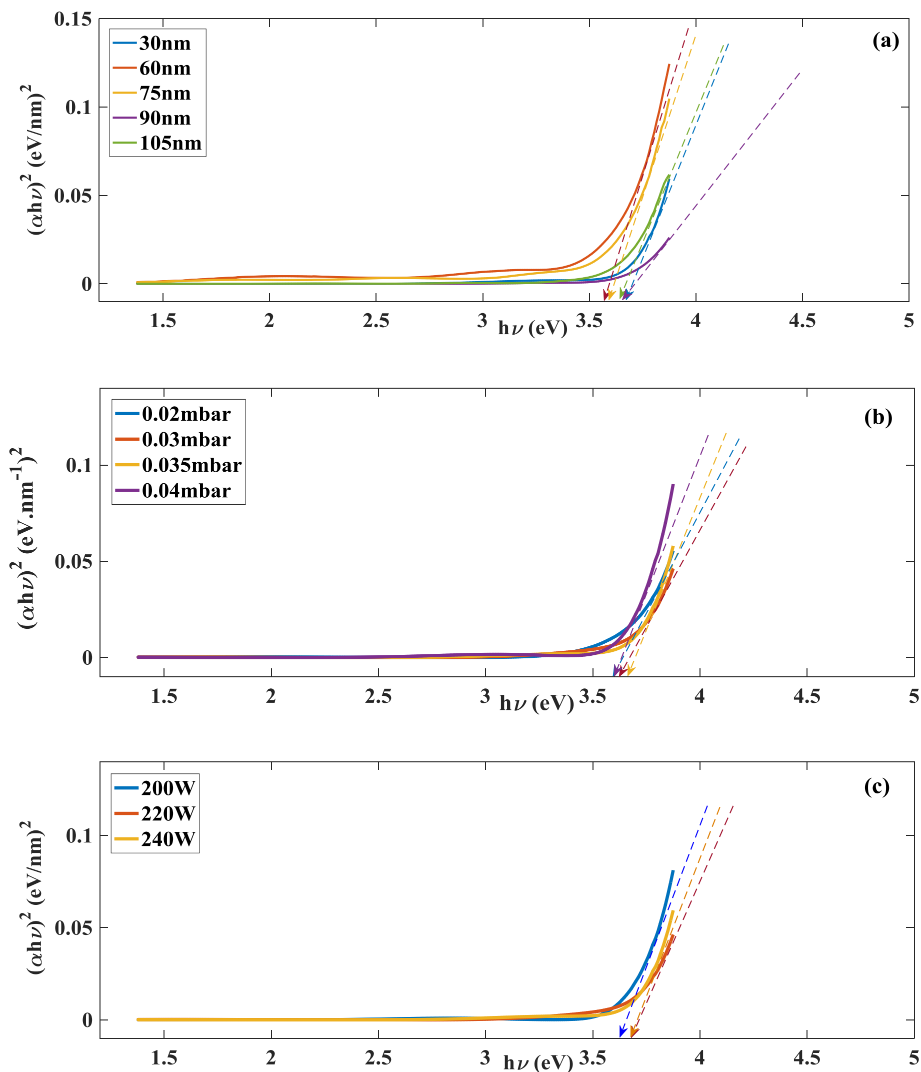

Fig. 12. Tauc's plot TiO_2 a) different thicknesses, b) under different sputtering pressures, and c) different sputtering powers.

TABLE VIII
The extracted band gap energy related to TiO_2 compact layer

Thickness(nm)	Pressure(mbar)	Deposion Power(W)	E_g (eV)
105	3.5×10^{-2}	240	3.635
90	3.5×10^{-2}	240	3.640
75	3.5×10^{-2}	240	3.587
60	3.5×10^{-2}	240	3.576
30	3.5×10^{-2}	240	3.664
30	2.0×10^{-2}	220	3.605
30	3.0×10^{-2}	220	3.647
30	3.5×10^{-2}	220	3.687
30	4.0×10^{-2}	220	3.623
30	3.5×10^{-2}	200	3.618

Using (VIII), the change of band gap energy versus different thicknesses, different chamber pressures and different deposition power are shown in Figs. 12-a, 12-b and, 12-c respectively.

As depicted by table (VIII) and Figs. 12-a, 12-b and, 12-c, the range of bands gap energy change is 3.618 to 3.687eV, showing that it depends highly on the process conditions and is compatible with other results [62]. Band gap energy of titanium dioxide deposited through DC magnetron sputtering method under different powers and pressures lies within the 3.20 to 3.28eV limits which is in line with the results of this study [63]. The bands gap energy of thin film of titanium dioxide with mixed phase has been reported in 3.58 to 3.75eV limit [43] which is in line with bands gap energy of this study in 3.576 to 3.687eV.

Usually, variations in bandwidth thickness occurs when quantum effects occur in the small nanometer ranges and deviates from the bandwidth thickness of the bulk state of the material, thus a change in energy band gap with a change in the thickness can be attributed to the grain size and pressure drop and grain boundary. As for the titanium dioxide layers made of constant thickness under different pressures and energies, changing the pressure or the power of the deposition causes a change in the amount of band gap energy which could be due to changes in the lattice parameters or the degree of the overlap between different titanium and oxygen orbitals. Therefore, the bands gap energy is dependent on the manufacture conditions including pressure and power, and changes in the conditions applied to the layer, and optimal laboratory situation can be designed according to the application type. Optical studies of thin films made under the conditions of this article using deposition method for optical devices with different applications are very promising. In summary each of the deposition parameters has an influence on the energy of the deposition particles

the geometry of the deposition chamber has to be taken into consideration as well. Partial pressure can influence the deposition mode (metal/oxide)/poisoning degree of the target [64]. Deposition pressure can influence the degree of ionization and the mean free path of sputtering and deposition atoms/ions. The power of the discharge plays a big part as well: by increasing it to a certain point, we can maximize the sputtering yield. It should be noted that too much power can lead to ion implantation, which should be avoided [44].

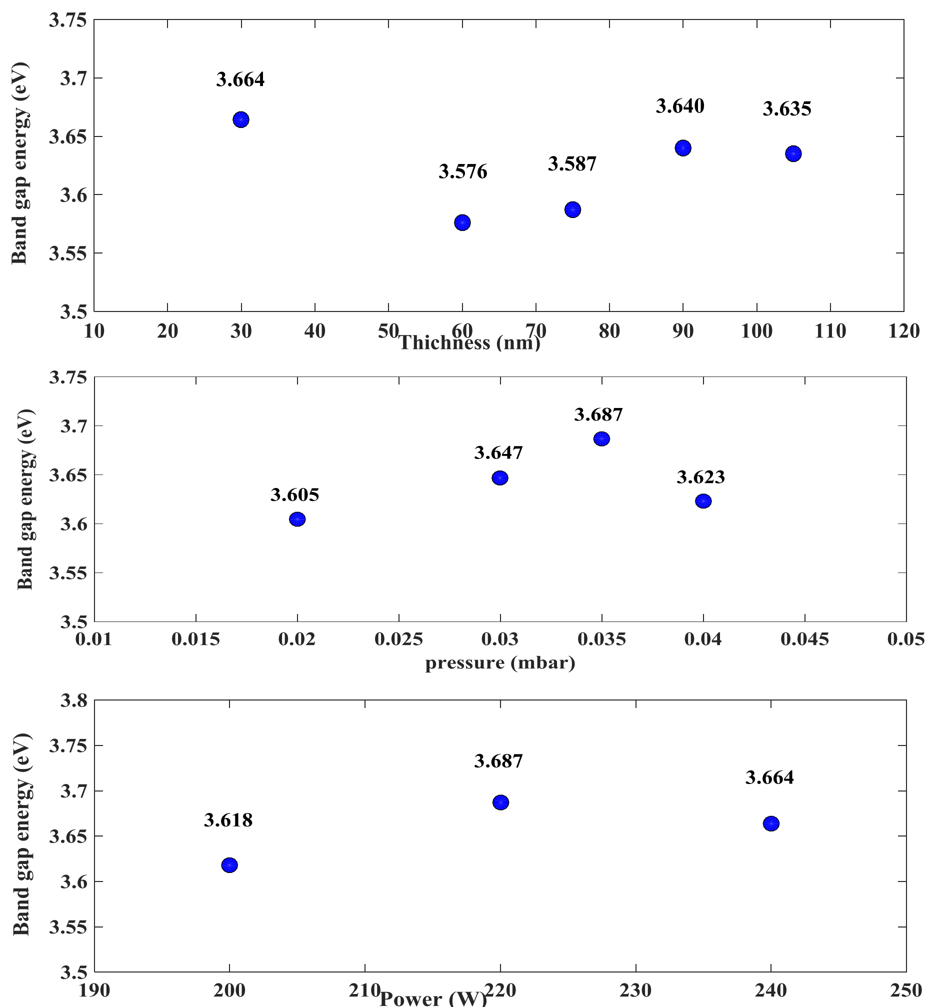

Fig. 12. Band gap energy's TiO_2 as a function of (a) different thicknesses, (b) different sputtering pressures, (c) different sputtering powers.

8. COCLUSION

In summary, we reported on the experimental study of the structural, electrical, electronic and optical properties of the TiO_2 thin films. It has been shown that in the making of titanium dioxide layer by radio frequency magnetron sputtering, different preparation conditions have a direct influence on the structure, lattice constants as well as the type of crystal phase. The X-ray analysis results revealed that the synthesized TiO_2 is composed of clusters of both anatase and rutile phases and all prepared layers are amorphous.

Reason behind may have been the effect of amorphous layers can be found in charged clusters. The experiment showed that for different thicknesses, the lattice structure was changed and consequently the lattice phase and constants were changed and therefore, the thickness change had no effect on crystallography, phase type and lattice structure, but it impacted on the lattice constants impressively. The calculated structural parameters are in close accordance with the published experimental work. It was also found that a change in pressure for thickness of 30nm had no effect on the crystallography, but changed the structure of the lattice, caused impurity to enter the lattice phase (Ti_3O_5 in the pressure of 3.5×10^{-2} mbar) and also changed the lattice constants.

Thickness 30 nm with different powers, it was found that the power change had no effect on crystallography but changed the lattice structure and also impurities in the lattice phase (Ti_3O_5 at 220 watt) and varies the lattice constants. The absorption of coefficient and the transmission rate of the layers were the evidence that these parameters are strongly dependent on the thickness change. Changes in power or pressure were observed, which sometimes affect the absorption of coefficients and the rate of transmittance of the titanium dioxide.

In layers with varied thicknesses, the highest level of transmission (the least absorption) of the light takes place within the wavelength of 400-600 nm. In making the layer with changing pressure and power, the maximum level of light transmission (least absorption) takes place first, within the wavelengths of 400-650nm and second, 450-700nm. Different preparation conditions, suitable for the type of application, can be designed to produce the mentioned layer. The band gap energy is strongly dependent on the thickness of the layer and varies with thickness.

Usually, bandwidth variations in thickness occur when quantum effects appear in the small nanometer ranges and deviates from the piled state of the material, thus, a change in band gap energy with a change in the thickness can

be attributed to the grain size, pressure drop and grain boundary. TiO_2 was made by changing the pressure or the power of the deposition. Furthermore, the amount of band gap energy was changed, which could be due to changes in the lattice parameters or the degree of overlap between different titanium and oxygen orbitals.

In conclusion, each of the deposition parameters has an influence on the energy of the deposition particles and one has to take into consideration the geometry of the deposition chamber as well. Partial pressure can influence the deposition mode (metal/oxide)/poisoning degree of the target. Deposition pressure can influence the degree of ionization and the mean free path of sputtering and deposition atoms/ions. The power of the discharge plays a big part as well: by increasing it to a certain point, we can maximize the sputtering yield, keeping in mind that too much power can lead to ion implantation, which is to be avoided [64]. With this band gap energy, the material is suitable for large optoelectronic applications.

ACKNOWLEDGMENTS

The author of the article appreciates and assistance the helps and cooperation of thin layer and analytical chemistry labs of physics, chemistry departments of Islamic Azad University of Marvdasht for preparing and spectroscopy of UV-VIS of the thin layer of TiO_2, and physics department X-ray scattering (XRD) laboratory of Shiraz University.

REFERENCES

[1] T. Minami, *Transparent conducting oxide semiconductors for transparent electrodes.* Semicond. Sci. Technol. 20(4) (2005) 35-44. Available: https://doi.org/10.1088/0268-1242/20/4/004.

[2] J.F. Wager, D.A. Kheszler, R.E. Persley, *Transparent Electronics*. Springer, (2008).

[3] D.K. Aswal, S.K. Gupta, *Science and Technology of Chemi resister Gas Sensors.* Nova Science Pub, (2007).

[4] J.F. Banifield, D.R. velben, D.J. Smith, *The identification of naturally occurring TiO_2 by structure determination using high-resolution electron microscopy,image simulation,and distance-least-squers refinement.* American. Mineralogist. 76(3-4) (1991) 343-353. Available: https://pubs.geoscienceworld.org/msa/ammin/article-abstract/76/3-4/343/42515/The-identification-of-naturally-occurring-TiO_2-B.

[5] V.A. Schwarz, S.D. Klein, R.H. Hornung, R. Knochenmuss, P. Wyss, D. Fink, U. Haler, H. Walt, *Laser in Surgery and Medicine.* Wiley, (2001) 252-256.

[6] C.M. Lampert, *Optical Coatings for Energy Efficiency and Solar Applications, in Durable innovative solar optical materials-the international challenge.* Houston, (1982).

[7] Q. Cai, J. Hu, *Effect of UVA/LED/TiO_2 Photocatalysis treated sulfamethoxazole and trimethoprim containing wastewater on antibiotic resistance development in sequencing batch reactors.* Water. Re. 140 (2018) 251-260. Available: https://doi.org/10.1016/j.watres.2018.04.053.

[8] H.R. Pouretedal, *Visible photocatalytic activity of co-dapted TiO_2/Zr, N nanoparticles in wastewater treatment of nitrotoluene sample.* J. Alloys. Compd. 735 (2018) 2507-2511. Available: https://doi.org/10.1016/j.jallcom.2017.12.018.

[9] G. Chiarello, M. Dozzi, E. Selli, *TiO_2 - based materials for Photocatalytic hydrogen production.* J. Energy. Chem. 26(2) (2017) 250-258. Available: https://doi.org/10.1016/j.jechem.2017.02.005.

[10] T. Jedsukontorn, T. Uneo, N. Saito, M. Hunsom, *Narrowing bandgap energy of defective black TiO_2 fabricated by solution plasma process and its photocatalytic activity on glycerol transformation.* Journal of Alloys and Compounds. 757 (2018) 188-199. Available: https://doi.org/10.1016/j.jallcom.2018.05.046.

[11] B. Richards, *Single-material TiO_2 double-layer antireflection coatings.* Sol. Energy Mater. Sol. Cells, 79(3) (2003) 369-390. Available: https://doi.org/10.1016/S0927-0248(02)00473-7.

[12] A. Majeed, J. He, L. Jiao, X. Zhong, Z. Sheng, *Surface properties and biocompatibility of nanostructured TiO_2 film deposited by RF magnetron sputtering.* Nanoscale Res. Lett. 10(56) (2015) 91. Available: https://doi.org/10.1186/s11671-015-0732-7.

[13] L. Bait, L. Azzouz, N. Saoula, N. Madaoui, *Influence of substrate bias voltage on the properties of TiO_2 deposited by radio-frequency magnetron sputtering on 304L for biomaterials applications.* Appl. Surf. Sci. 395 (2017) 72-77. Available: https://doi.org/10.1016/j.apsusc.2016.07.101.

[14] R.E. Krebs, *The History and use of our Earths Chemical Elements.* GreenWood, Press, 2006.

[15] S. Ikhmayies, *Advanced in silicon solar cells.* Springer, (2008).

[16] S.M. Manakov, K.K. Dikhanbaev, M.A. Ikhankyzy, T.I. Taurbayev, Z.A. Mansurov, A.B. Lesbayev, Y. Sagidolda, *Light Trapping Enhancement in Gallium Arsenide Solar Cells, Journal of Nanoelectronics and Optoelectronics.* Journal of Nanoelectronics and Optoelectronics. 9(4) (2014) 511-514. Available: https://doi.org/10.1166/jno.2014.1626.

[17] U. MANDADAPU, S.V. VEDANAYAKAM, K. TYAGARAJAN, M. RAJA REDDY, B.J. BABU, *OPTIMISATION OF HIGH EFFICIENCY TIN HALIDE PEROVSKITE SOLAR CELLS USING SCAPS-1D.* International Journal of Simulation & Process Modelling. 13(3) (2018) 221-227. Available: https:// doi/abs/10.1504/IJSPM.2018.093097.

[18] T. Zdanowicz, T. Rodziewicz, M. Zabkowska-Waclawek, *Theoretical analysis of the optimum energy band gap of semiconductors for fabrication of solar cells for applications in higher latitudes locations.* Solar Energy Material & Solar Cells. 87(1-4) (2005) 757-769. Available: https://doi.org/10.1016/j.solmat.2004.07.049.

[19] P.M. Sommeling, B.C. Oregan, R.P. Haswell, H.J.P. Smith, N.J. Baker, J.J.T Smits, J.M. Kroon, J.A.M. Van Roosmalen, *Influence of a $TiCL_4$ post-treatment on nanocrystalline TiO_2 films in dye-sensitized solar cells.* J. Phys. Chem. B, 110(39) (2006) 19191-19197. Available: https:// doi/abs/10.1021/jp061346k.

[20] J. Hu, P. Liu, M. Chen, S. Li, Y. Yang, *Synthesis and first principle calculation of TiO_2 rutile nanowire electrodes for dye-sensitized solar cells.* Int. J. ElectroChem. Sci. 12 (2017) 9725-9735. Available: http://electrochemsci.org/doi:10.20964/2017.10.47.

[21] A. Zabon, S.T. Aruna, S. Tirosh, B.A. Gregg, Y. Mastai, *The effect of the preparations condition of TiO_2 colloids on their surface structures.* J. Phys. Chem. B**.** 104(17) (2000) 4130-4133. Available: https://doi.org/10.1021/jp993198m.

[22] D. Reyes-Coronado, G. Rodriguez-Gattorno, M.E. Espinosa-Pesqueira, C. Cab, R.D. De Coss, G. Oskam, *Phase-pure TiO_2 nanoparticles: anatase,brookite and rutile.* Nanotechnology. 19 (2008) 145605. Available: https://doi.org/10.1088/0957-4484/19/14/145605.

[23] Z. Lin, C. Jiang, C. Zhu, J. Zhang, *Development of inverted organic solar cells with TiO_2 interface layer by using low-term-perature atomic layer*

deposition. ACS Appl. Mater. Interfaces. 5(3) (2013) 713-718. Available: https://doi.org/10.1021/am302252p.

[24] M.N. Islam, T.B. Ghosh, K.L. Chopra, H.N. Acharya, *XPS and X-ray diffraction studies of aluminum-doped zinc oxide transparent conducting films.* Thin Solid Films. 280(1-2) (1996) 20-25. Available: https://doi.org/10.1016/0040-6090(95)08239-5.

[25] J. Yu, X. Zhao, J. Du, W. Chen, *Preparation, microstructure and photocatalytic activity of the porous TiO_2 anatase coating by sol-gel processing,* J. Sci. Technol. 17 (2007) 163-171. Available: https://doi.org/10.1023/A:1008703719929.

[26] J. Hu, R.G. Gordan, *Textured aluminum‐ doped zinc oxide thin films from atmospheric pressure chemical‐ vapor deposition.* J. Appl. Phys. 71(2) (1992) 880. Available: https://doi.org/10.1063/1.351309.

[27] J.-H. Kim, S. Lee, H.-S. Im, t*he effect of target density and its morphology on TiO_2 thin films grown on Si (100) by PLD.* Appl. Surf. Sci. 151(1-2) (1999) 6-16. Available: https://doi.org/10.1016/S0169-4332(99)00269-X.

[28] C.H. Heo, S.B. Lee, J.H. Boo, *Deposition of TiO_2 thin films using RF magnetron sputtering method and study of their surface characteristics.* Thin solid films. 475(1-2) (2005) 183-188. Available: https://doi.org/10.1016/j.tsf.2004.08.033.

[29] T. Minami, H. Sato, K. Ohashi, T. Tomofuji, S. Takata*, Conduction mechanism of highly conductive and transparent zinc oxide thin films prepared by magnetron sputtering.* J. Cryst. Growth. 117(1-4) (1992) 370-374. Available: https://doi.org/10.1016/0022-0248(92)90778-H.

[30] X. Chen, S.S. Mao, *Titanium dioxide nanomaterials: synthesis, properties, modifications and applications.* ACS Publications. 107(7) (2007) 2891-2959. Available: https://doi.org/10.1021/cr0500535.

[31] A. Hadipour, D. Cheyns, P. Heremans, B.P. Rand, *Electrode considerations for the optical enhancement of organic bulk heterojunction solar cells.* Adv. Energy. Mater. 1 (2011) 930-935. Available: https://doi.org/10.1021/cr0500535.

[32] J.T.W. Wang, J.M. Ball, E.M. Barea, A. Abate, J.A. Alexander-Webber, J. Huang, M. Saliba, I. More-Sero, J. Bisquert, H.J. Snaith, R.J. Nicholas*, Low-temperature processed electron collection layers of graphene/TiO_2 nanocomposites in thin film perovskite solar cells.* Nano. Lett. 14(2) (2013) 724-730. Available: https://doi.org/10.1021/nl403997a.

[33] U.J. Krull, M. Thompson, *Encyclopedia of Physical science and Technology: Analytical Chemistry.* 3rd, Academic Press, (2001).

[34] J. Tauc, *Optical properties and electronic structure of amorphous Ge and Si.* Materials Research. Bulletin. 3(1) (1968) 37-46. Available: Available: https://doi.org/10.1016/0025-5408(68)90023-8.

[35] Y. Wang, L. Zhang, K. Deng, X. Chen, Z. Zou, *Low temperature synthesis and photocatalytic activity of rutile TiO_2 nanorode superstructures.* J. Phys. Chem. C. 111(6) (2007) 2709-27014. Available: https://doi/abs/10.1021/jp066519k.

[36] K. Bange, C.R. Ottermann, O. Anderson, U. Jeschkowski, R.M. Laube Feile, *Investigations of TiO_2 films deposited by different techniques.* Thin Solid Films. 197(1-2) (1991) 279-285. Available: https://doi.org/10.1016/0040-6090(91)90238-S.

[37] L. Williams, M.D.W. Hess, *Structural properties of titanium dioxide films deposited in an rf glow discharge.* Journal of Vacuum Science & Technology. 1(4) (1983) 1810. Available: https://doi.org/10.1116/1.572220.

[38] M.H. Suhail, G. Mohan Rao, S. Mohan, *Dc reactive magnetron sputtering of titanium- structural and optical characterization of TiO_2 films.* J. Appl. Phys. 71(3) (1992) 1421. Available: https://doi.org/10.1063/1.351264.

[39] S. Schiller, G. Beister, W. Sieber, G. Schirmer, E. Hacker, *Influence of Deposition Parameters on the Optical and Structural Properties of TiO_2 Films Produced by Reactive DC Plasmatron Sputtering.* Thin Solid Films. 83(2) (1981) 239-245. Available: https://doi.org/10.1016/0040-6090(81)90673-8.

[40] W.T. Pawlewicz, R. Busch, *Reactively sputtered oxide optical coatings for inertial confinement fusion laser components.* Thin Solid Films. 63(2) (1979) 251-256. Available: https://doi.org/10.1016/0040-6090(79)90023-3.

[41] D.R. Mardare, *The influence of heat treatment on the optical properties of titanium oxide thin films.* Materials Letters. 56(3) (2002) 210-214. Available: https://doi.org/10.1016/S0167-577X(02)00441-X.

[42] Y.-Q. Hou, D.M. Zhuang, M.Z. Zhang, M.S. Wu, *Influence of annealing temperature on the properties of titanium oxide thin film.* Applied Surface Science. 218(1-4) (2003) 98-106. Available: https://doi.org/10.1016/S0169-4332(03)00569-5.

[43] P.B. Nair, V.B. Justinvictor, G.P. Daniel, K. Joy, V. Ramakrishnan, P.V. Thomas, *Optical parameters induced by phase transformation in RF magnetron sputtered TiO_2 nanostructured thin films.* Applied. Surface. Science. 24(3) (2014) 218-225. Available: https://doi.org/10.1016/j.pnsc.2014.05.010.

[44] [44] M.C. Liao, H. Niu, G. Chen, *Effect of sputtering pressure and post-annealing on hydrophilicity of TiO_2 thin films deposited by reactive magnetron sputtering.* Thin Solid Film. 518(24) (2010) 7258-7262. Available: https://doi.org/10.1016/j.tsf.2010.04.106.

[45] A. Wiatrowski, M. Mazur, A. Obstarczyk, D. Wojcieszak, D. Kaczmarek, J. Morgiel, D. Gibson, *Comparison of the Physicochemical Properties of TiO_2 Thin Films Obtained by Magnetron Sputtering with Continuous and Pulsed Gas Flow.* Coatings. 8(11) (2018) 412. Available: https://doi.org/10.3390/coatings8110412.

[46] O.-G. Simionescu, C. Romanit, O. Tutunaru, V. Ion, O. Buiu, A. Avram, *RF Magnetron Sputtering deposition of TiO_2 Thin Films in a Small Continouos Oxygen Flow Rate*. coatings. 9(7) (2019) 442. Available: https://doi.org/10.3390/coatings9070442.

[47] M.Soussi, A. Ait hssi, M.Boujnah, K. Abouabbasi, A. Asbayou, A. Elfanaoui, R. Markazi, A. Ihlal, K. Bouabid, *Electronic and Optical Properties of TiO_2 Thin Films: Combined Experimental and Theoretical Study.* Journal of Electronic Materials. 50 (2021) 4497-4510. Available: https://doi.org/10.1007/s11664-021-08976-8.

[48] N.N. Anua, R. Ahmed, A. Shaari, M.A. Saeed, B.U. Haq, S. Goumri-Said, *Non-local exchange correlation functionals impact on the structural, electronic and optical properties of III–V arsenides.* Semicond. Sci. Technol. 28 (2013) 105015. Available: https://doi.org/10.1088/0268-1242/28/10/105015.

[49] S. Di Mo, W.Y. Ching, *Electronic and optical properties of three phases of titanium dioxide: Rutile, anatase, and brookite.* Phys. Rev. B. 51(19) (1995) 13023. Available: https://doi.org/10.1103/PhysRevB.51.13023.

[50] C. Lee, X. Gonze, *Dielectric constants and Born effective charges of TiO_2 rutile.* Phys. Rev. B. 49 (1994) 14730. Available: https://doi.org/10.1103/PhysRevB.49.14730.

[51] M.M. Islam, T. Bredow, A. Gerson, *Electronic properties of oxygen-deficient and aluminum-doped rutile TiO_2 from first principles.* Phys. Rev. B. 76(4) (2007) 1. Available: https://doi.org/10.1103/PhysRevB.76.045217.

[52] F. Tran, P. Blaha, K. Schwarz, *Band gap calculations with Becke–Johnson exchange potential.* J. Phys. Condens. Matter, 19 (2007)196208. Available: https://doi.org/10.1088/0953-8984/19/19/196208.

[53] A. Elfanaoui, E. Elhamri, L. Boulkaddat, A. Ihlal, K. Bouabid, L. Laanab, A. Taleb, X. Portier, *Optical and structural properties of TiO_2 thin films prepared by sol–gel spin coating.* Int. J. Hydrogen Energy. 36 (2011) 4130-4133. Available: https://doi.org/10.1016/j.ijhydene.2010.07.057.

[54] N. J. Shivaramu, K. R. Nagabhushana, B.N. Lakshminarasappa, F. Singh, *Ion beam induced luminescence studies of sol gel derived Y_2O_3:Dy^{3+} nanophosphors.* Journal of Luminescence. 169(B) (2016) 627-634. Available: https://doi.org/10.1016/j.jlumin.2015.07.054.

[55] M. K. Woka, L. Ottaviano, J. Szuber, *AFM study of the surface morphology of L-CVD SnO_2 thin films.* Thin Solid Films. 515(23) (2007) 8328-8331. Available: https://doi.org/10.1016/j.tsf.2007.03.035.

[56] A. E. Lita, J. E. Sanchez Jr., *Characterization of surface structure in sputtered Al films: Correlation to microstructure evolution.* J. Appl. Phys. 85(2) (1999) 876. Available: https://doi.org/10.1063/1.369206.

[57] D. Raoufi, A. Kiasatpour, H.R. Fallah, A.S.H. Rozatian, *Surface characterization and microstructure of ITO thin films at different annealing temperatures.* Appl. Surf. Sci. 253(23) (2007) 9085-9090. Available: https://doi.org/10.1016/j.apsusc.2007.05.032.

[58] H.C. Ward, T.R. Thomas, *Rough Surfaces*, Ed., Longman, London, 1982.

[59] G. B. Williamson, R. C. Smallman, *III. Dislocation densities in some annealed and cold-worked metals from measurements on the X-ray Debye Scherrer spectrum.* Phil. Mag. 1(1) (1956) 34-46. Available: https://doi.org/10.1080/14786435608238074.

[60] B.R. kumar, T.S. Rao, *AFM Studies on surface morphology, topography and texture of nanostructured zinc aluminium oxide thin films*, Digest Journal of Nanomaterials and Biostructures. 7(4) (2012) 1881-1889.

[61] K. Wysocka, A. Ulatowska, J. Bauer, I. Holowacz, B. Savu, G. Stanciu, *Optica Applicata.* 38 (2008) 130. Available: https://doi.org/10.17482/uumfd.309657.

[62] N.P. Poddar, S.K. Mukherjee, *Anatase phase evolution and its stabilization in ion beam sputtered TiO_2 thin films,* Thin Solid Films. 666 (2018) 113-120. Available: https://doi.org/10.1016/j.tsf.2018.09.038.

[63] P. Singh, D. Kaur, *Room temperature growth of nanocrystalline anatase TiO_2 thin films by dc magnetron sputtering*. Physica. B: Condensed Matter. 405(5) (2010) 1258-1266. Available: https://doi.org/10.1016/j.physb.2009.11.061.

[64] B.N.Chapman, *Sputtering InGlow Discharge Processes—sputtering and Plasma Etching*. Wiley, NewYork, NY, USA, (1980) 177–296.